Acta Cryst. (1995). A51, 124–129

Thermal Diffuse Scattering in Time-of-Flight Neutron Diffraction Studies on SBN and TSCC Single Crystals

BY F. PROKERT

Research Center Rossendorf, IIM, PB 510119, 01314 *Dresden, Germany*

AND B. N. SAVENKO AND A. M. BALAGUROV

Joint Institute of Nuclear Research, LNP, Dubna, Russia

(*Received* 16 *February* 1994; *accepted* 1 *August* 1994)

Abstract

Thermal diffuse scattering (TDS) from single crystals of barium strontium niobate (SBN) and from a partly deuterated single crystal of tris(sarcosine) calcium chloride (TSCC) measured on the time-of-flight (TOF) Laue single-crystal diffractometer DN-2/IBR-2, Dubna, Russia, are presented. Various characteristic distributions of the TDS were measured and could be interpreted for the elastically (nearly) isotropic SBN crystals as well as for the anisotropic TSCC sample in accordance with the theory. The velocities of sound propagation are determined in both cases. Temperature-dependent changes of the TDS are qualitatively analysed for SBN crystals.

Introduction

In connection with the study of single crystals at pulsed neutron sources, questions concerning the separation of the components of diffuse scattering from the Bragg scattering have been the subject of increased interest. In two basic papers (Willis, 1986; Schofield & Willis, 1987), the nature of thermal diffuse scattering (TDS) close to the Bragg reflections in time-of-flight (TOF) neutron diffraction was discussed in detail. The experimental data from pyrolytic graphite (Willis, Carlile, Ward, David & Johnson, 1986) and from single crystals of barium fluoride (Carlile, Keen, Wilson & Willis, 1992) and calcium fluoride (Carlile & Willis, 1989) agree with the theoretical predictions. These experiments were performed at the ISIS pulsed neutron facility on the high-resolution powder diffractometer (HRPD) in near back scattering as well as on the single-crystal diffractometer SXD.

In phase-transition studies, performed at the pulsed reactor IBR-2, on single crystals of strontium barium niobate (SBN) (Balagurov, Prokert & Savenko, 1987) and of tris(sarcosine) calcium chloride (TSCC), the peak profile of some Bragg reflections indicate that the intensities are clearly influenced by phonon scattering. Especially in the case of SBN, the latter must be separated from a more-specific diffuse (quasi-)elastic component that occurs at the diffuse ferroelectric phase transition (PT). For that reason, we decided to study the effects of TDS in SBN and TSCC in more detail.

Review of theoretical aspects

As shown in the basic papers, TDS from the long-wavelength acoustic modes in single crystals in the TOF Laue technique is characterized by the ratio, β, of the velocity of sound c_s to the neutron velocity v_n. Because the peak positions are determined in this technique by the neutron velocity, the ratio β varies for different reflections and the TDS around the Bragg peaks may change its profile drastically.

There are three regions to be considered in calculating the nature of this scattering.

1. If $v_n > c_s$, the TDS rises to a maximum at the Bragg peak position and scattering is allowed at all points in the reciprocal space.

2. If $c_s > v_n > c_s \cos\theta$, where θ is half the scattering angle, the TDS rises to a steep maximum on either side of the Bragg peak at θ_B and scattering between these maxima is forbidden.

3. If $c_s \cos\theta > v_n$, there is one maximum only, and this is associated with phonon emission for $\theta > \theta_B$ and phonon absorption for $\theta < \theta_B$.

The third region, already studied for barium fluoride on SXD at ISIS, is investigated here for SBN single crystals, whereas the TSCC measurements in this paper were evaluated mainly for data from the second region. The theoretical predictions could be tested using the elastic constants that are known for SBN as well as for TSCC crystals almost completely.

The following notations (as given by Willis, 1986) are used here. E_0 and E: initial and final energies of neutron; **B**: reciprocal-lattice vector; **e**(j**q**): polarization vector of excited mode of vibration (j**q**); $\mathbf{k}_0$ and **k**: initial and final wave vectors of a neutron; N: number of unit cells in the crystal; **q**: wave vector of the normal mode; **Q**: scattering

vector ($= \mathbf{k} - \mathbf{k}_0$); $\omega_j(\mathbf{q})$: frequency of the normal mode ($j\mathbf{q}$).

The phonon intensity for absorption ($\varepsilon = -1$) and emission ($\varepsilon = +1$) is given by

$$\left(\frac{d\sigma}{d\Omega}\right)^{\text{inel}}_{\text{coh},\varepsilon} = \left(\frac{k}{k_0}\right)\left(\frac{N}{2}\right)\sum_j \{[n_j(\mathbf{q}) + \tfrac{1}{2} + \varepsilon\tfrac{1}{2}]/\omega_j(\mathbf{q})\} \times |G_j(\mathbf{Q})|^2 |J_\varepsilon|^{-1}. \quad (1)$$

Here, $G_j(\mathbf{Q})$, the so-called *one-phonon structure factor*, and $n_j(\mathbf{q})$, the quantum number of phonon modes, are given by

$$n_j(\mathbf{q}) = \{\exp[\hbar\omega_j(\mathbf{q})/k'_B T] - 1\}^{-1}, \quad (2)$$

where k'_B is Boltzmann's constant and T is the absolute temperature. From (1) and (2), it follows that at sufficiently high temperatures [if the additional contribution to $n_j(\mathbf{q})$ for phonon emission is negligible] the scattering cross section for annihilation and creation differ mainly by the Jacobian term $|J_\varepsilon|^{-1}$.

In the study of acoustic phonon scattering, one has to consider the elastic anisotropy of the crystals. Crystals are elastically anisotropic, for isotropic sound propagation only, if additional relations between the elastic constants are fulfilled, *i.e.* the phase velocity, c_c, equals the group velocity, c_g. As shown by Schofield & Willis (1987), the anisotropy enters into the basic formulae with the substitution of β by $\beta_g = c_g/v_n$.

Experimental

The experiments were carried out on the single-crystal TOF spectrometer DN-2 installed at the pulsed reactor IBR-2 of the JINR in Dubna. The instrument has a long primary flight path, $L_0 = 23.75$ m, from moderator to sample (partly within a neutron guide) and a short secondary one L_1 from sample to detector (1.05 m in the set-up used). With a one-dimensional position-sensitive detector, diffraction patterns are taken from a sectorial area ($\Delta 2\theta = \pm 11.9°$) of the reciprocal space around the chosen direction. The central detector position 2θ was fixed at about 90°. As a consequence of $L_1 \ll L_0$, the contribution from the secondary flight path is negligible in the differences (Δt) between the flight time for phonon scattering (t) and the time for Bragg scattering (t_B).

Results from barium strontium niobate mixed crystals

At room temperature (RT) in the composition range $0.75 \geq x \geq 0.25$, the mixed crystals $Sr_xBa_{1-x}Nb_2O_6$ (SBN-X, $X = 100x$) are (pseudo-)tetragonal and have tungsten-bronze structure. [The incommensurate modulation and weak orthorhombic distortions of the structure (Balagurov, Prokert & Savenko, 1987) may be neglected here.] There are five formula units in the unit cell ($a \simeq 12.43$, $c \simeq 3.91$ Å; density of SBN-50 is ~ 5.5 g cm^{-3}). Crystals of various compositions ($0.50 \leq x \leq 0.75$) were investigated between 15 and 773 K in a refrigerator cryostat and a furnace, respectively.

In analogy to the Cauchy relation for cubic crystals for elastic isotropy around the c axis of a tetragonal crystal, the relation $c_{11} - c_{12} - 2c_{66} = 0$ must be fulfilled. The relevant stiffness constants are known from piezoelectric resonance methods (Liu & Cross, 1977; Liu, 1978) and phonon dispersion measurements (Prokert, 1982). Despite considerable differences between the two sets of elastic constants, the isotropy relation is nearly fulfilled for both. Complete elastic isotropy requires additional relations between the six independent nonzero elastic constants. However, from numerical calculations (using formulae given by Every, 1980), it follows that in the two relevant scattering planes [(010) and (1$\bar{1}$0)] the phase velocity of the two quasi-transverse modes is only weakly directional dependent. In the worst case of our data sets, the change of velocity does not exceed 12% for the mixed mode and 1% for the quasi-pure quasi-transverse one, respectively. Near the high-symmetry directions, at which an exact decision between longitudinal ($j = 1$) and transverse modes ($j = 2, 3$) exists, and for the given vertical divergence ($\leq 20'$) of the neutron beam, the latter mode will dominate in the phonon scattering because of the polarization term $[\mathbf{Q} \cdot \mathbf{e}(j\mathbf{q})]$ in the one-phonon structure factor.

The measurements on various samples have shown that the strong 002 reflections of SBN-X recorded in the zones [1$\bar{1}$0] and [100], respectively, are strongly influenced by thermal diffuse scattering. This is illustrated in Fig. 1 on a sample of SBN-61 for a scan in the (100) plane. Fig. 2 shows the TDS in a contour plot of intensity measured at room temperature (RT) on a SBN-50 sample around the 002 reciprocal-lattice point. For a given $\Delta 2\theta$, the TDS occurs only on one side of the Bragg peak (t_B, $2\theta_B$). As expected from the theory for the case $c_s \cos\theta > v_n$, the TDS appears at shorter times of flight than t_B if $2\theta < 2\theta_B$ (phonon emission) and at longer times if $2\theta > 2\theta_B$ (phonon absorption). By a variation of the β parameter, various curves were calculated for the central position of the TDS, using the relation

$$\frac{\Delta t}{\Delta 2\theta} = \tfrac{1}{2} t_B \frac{\tan\theta}{\beta^2 \cos^2\theta - 1} \quad (3)$$

(Carlile, Keen, Wilson & Willis, 1992), with $\Delta t = t - t_B$ and $\Delta 2\theta = 2\theta - 2\theta_B$. From the curve fitting (with curve C), a phonon velocity of $c_s = 2.90$ km s^{-1} was approximated. This value also fits the TDS pattern measured at RT on SBN-61 and SBN-70 single crystals around 002. This fitted phonon velocity is not far from the calculated one, $c_s^{\text{calc}} = 3.16$ km s^{-1} determined for

the elastically isotropic case from the relevant c_{44} constant.

Around the 001 Bragg reflection in SBN, the contributions of phonon scattering were found to be quite small. The TDS at RT is obscured by other kinds of diffuse scattering.

The dependence of the TDS on temperature is demonstrated in Fig. 3. The enhancement of TDS comes from the increased occupation number $n_j(\mathbf{q})$ (2), which clearly overcompensates for the influence of the Debye–Waller term in the one-phonon structure factor $G_j(\mathbf{Q})$. From $q \simeq 10^{-2} \times |\mathbf{B}^{(002)}|$, we have a phonon energy $\hbar\omega_j(\mathbf{q}) \simeq 0.5$ meV and, for temperatures 293 and 700 K, we get values of $n_j^{293} \simeq 60$ and $n_j^{700} \simeq 120$, respectively.

Comparing the intensities for phonon annihilation ($\varepsilon = -1$) and phonon creation ($\varepsilon = +1$) in SBN around 002, one sees higher values for annihilation in agreement with the theory. Then, as shown by Willis (1986) for elastically isotropic material, the Jacobian becomes

$$J_\varepsilon = 1 + \varepsilon\beta \tag{4}$$

and

$$\frac{(\mathrm{d}\sigma/\mathrm{d}\Omega)^{\varepsilon=-1}}{(\mathrm{d}\sigma/\mathrm{d}\Omega)^{\varepsilon=+1}} = \frac{|J_{-1}|^{-1}}{|J_{+1}|^{-1}} = \frac{|1-\beta|^{-1}}{|1+\beta|^{-1}} = \frac{|1+\beta|}{|1-\beta|}. \tag{5}$$

With the relevant value $\beta_{(002)}^{\mathrm{SBN}} \simeq 2$ therefore we get a ratio of ~ 3.

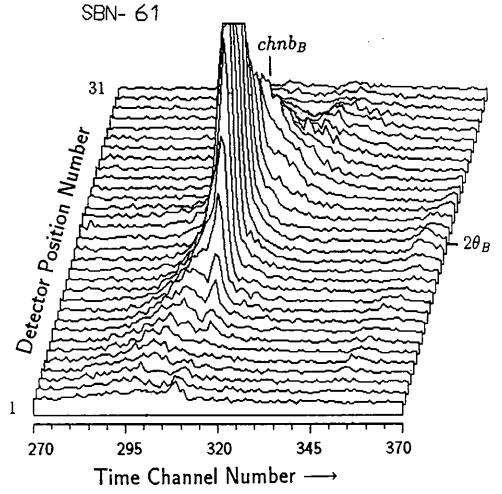

Fig. 1. 3D plot of intensity around the 002 reflection (in the [100] zone) of strontium barium niobate mixed crystal SBN-61 showing phonon wings around the Bragg peak at $2\theta_B = 90°$ and at channel number $\mathrm{chn}b_B$ ($\Delta 2\theta$ range ±6.1°, time channel width $\mathrm{ch}_w = 64$ μs).

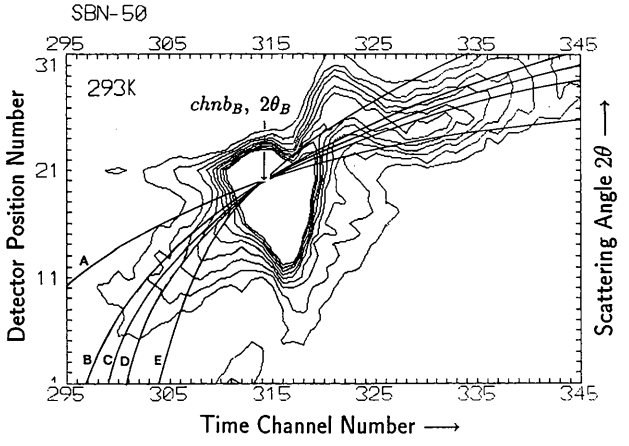

Fig. 2. Contour plot of the intensity around the 002 reflection (in the [1$\bar{1}$0] zone) of SBN-50. The detector positions 1–32 cover the 2θ range 86.3–98.5°. Time channel width $\mathrm{ch}_w = 64$ μs. Bragg peak t_B, $2\theta_B$ at channel number, $\mathrm{chn}b_B = 315$, $2\theta_B = 92.4°$. The curves *A*, *B*, *C*, *D* and *E* are calculated for $c_s = 2.5$, 2.8, 2.9, 3.0 and 3.3 km s^{-1}.

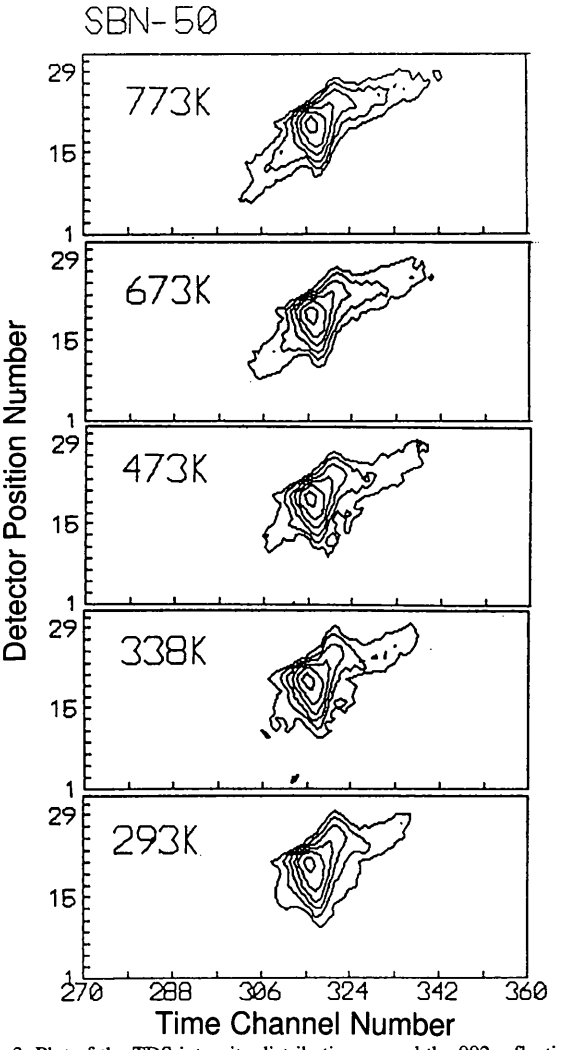

Fig. 3. Plot of the TDS intensity distribution around the 002 reflection (in the [1$\bar{1}$0] zone) of SBN-50 at RT and at 773, 673, 473 and 338 K ($2\theta_B = 90°$; 2θ range 78.5–101.5°; $\mathrm{ch}_w = 64$ μs).

Results from partly deuterated tris(sarcosine) calcium chloride

At RT, in the paraelectric phase TSCC is orthorhombic (*Pnma*) and ferroelastic with four formula units $(CH_3NHCH_2COOH)_3 \cdot CaCl_2$ in the unit cell ($a = 9.156$, $b = 17.460$, $c = 10.265$ Å; density of undeuterated TSCC = 1.533 g cm^{-3}). The axial ratio b/c is $\sim 3^{1/2}$ and viewed along the a axis the crystal structure is pseudohexagonal. Below 127 K, owing to a second-order PT, TSCC is orthorhombic ($Pn2_1a$) and uniaxial ferroelectric (Sawada, Makita & Takagi, 1977). The studied single crystal was partly deuterated [(CH_2) groups to 25% and both groups (NH) and (COOH) to 75%] to reduce the incoherent neutron scattering. Nevertheless, small coherent effects are partly obscured by a considerable background.

The measurements were performed at RT and below the PT at 130 K. The scans in the [001] zone were directed along the a^* and b^* axes, respectively. In the diffraction patterns of TSCC, the phonon contributions are very pronounced in the above-discussed second region of neutron velocity. A typical distributions of TDS around a Bragg peak is shown in Fig. 4.

Some of the nine elastic constants (in units of 10^{10} Nm^2: $c_{11} = 3.75$, $c_{22} = 4.24$, $c_{12} = 2.23$, $c_{66} = 0.64$ and $c_{44} + c_{55} = 1.6$) are known from Brillouin spectroscopy (Prokhorova, Smolensky, Siny, Kuzminov, Mikvabia & Arndt, 1980). For an estimation of the elastic anisotropy, we make use of the pseudohexagonal symmetry. The elastic constant matrix then corresponds to the matrix of the tetragonal group with $c_{66} = \frac{1}{2}(c_{11} - c_{12})$.

Numerical calculations (again after Every, 1980) show that the anisotropy of the phase velocities of the two pseudotransverse modes depends significantly on the hexagonal c_{12} constant and that in the relevant (orthorhombic) [001] zone *both* of these velocities vary distinctly with the propagation direction.

In the anisotropic case, the ratio β is no longer independent of propagation direction. If ζ is the angle between reciprocal-lattice vector **B** and phonon vector **q**, the phonon frequency is given by

$$\omega(\mathbf{q}) = c(\zeta)q. \tag{6}$$

The group velocity of the phonon, c_g, given by the gradient of $\omega(\mathbf{q})$, has components $c(\zeta)$ along the direction of **q** and $c'(\zeta)$ perpendicular to this direction. Hence, there is an angle α between the direction of group propagation and the phonon wave vector. Thus, an edge in the TOF spectrum corresponds to the creation or annihilation of a phonon of a group velocity c_g whose direction of (group) propagation relative to the Bragg direction is given by equation (62) of Schofield & Willis (1987).

$$\zeta + \alpha = \theta - \theta_B + \arctan(T_{\tau,\theta} / \sin\theta_B) \tag{7}$$

with

$$T_{\tau,\theta} = \tau \sin\theta - \cos\theta_B \tag{8}$$

and

$$\tau \equiv \tau(\zeta) = (1/t_B)[\Delta t(\zeta) / \sin\Delta\theta]. \tag{9}$$

These relations and equation (63) of Schofield & Willis (1987), adapted for the experimentally given flight paths L_0 and L_1,

$$\begin{aligned}\beta_g = {} & [1 - 2\tau \sin\theta\cos\theta_B + \tau^2 \sin^2\theta]^{1/2} \\ & \times \{|(0.959)\sin\theta_B \sin\theta + \cos\theta_B \cos\theta \\ & - \tau \sin\theta\cos\theta|\}^{-1}\end{aligned} \tag{10}$$

were used for the determination of phonon-group direction and velocity c_g, respectively, from the measured edges of the window. The results for $\Delta\theta = -3.22°$ are compiled in Tables 1 and 2 for the TOF scan along the b axis and the a axis, respectively. The latter was taken at 123 K in the ferroelectric phase. In both cases, the results were checked for the position $\Delta\theta = +3.22°$. Within an uncertainty of 5%, the same values were found, but with an exchanged sign of ε (excitations of phonons change from absorption to emission and *vice versa*, respectively).

Fig. 5 shows a typical contour plot of the TDS around a Bragg reflection of the second region ($c_g > v_n > c_g \cos\theta$). The recalculated curves for the edge positions in Fig. 5 fit the measured data acceptably only if two different velocities are used. This agrees with the fact that in the anisotropic case the two edges of the window correspond in general to different phonon propagation directions with different group velocities

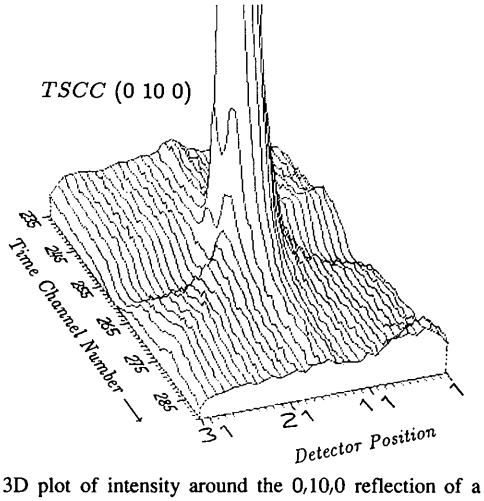

Fig. 4. 3D plot of intensity around the 0,10,0 reflection of a partly deuterated TSCC crystal showing edges of a 'wavelength window' of the TDS near the Bragg peak at $2\theta_B = 89.8°$ ($\Delta 2\theta$ range ±5.9°, $ch_w = 64$ μs).

Table 1. *Group velocities in TSCC at RT from edges of phonon emission* ($\varepsilon = +1$) *and absorption* ($\varepsilon = -1$) *in TOF scans along the b direction*

$\theta = 44.8°$, $\Delta\theta = -3.22°$

		$\varepsilon = +1$			$\varepsilon = -1$		
hkl	v_n (km s^{-1})	β_g	c_g (km s^{-1})	$\zeta + \alpha$	β_g	c_g (km s^{-1})	$\zeta + \alpha$
0 16 0	2.569	1.269	3.259	−20.7	1.041	2.674	117.6
0 12 0	1.927	1.195	2.301	−26.1	1.045	2.013	116.1
0 10 0	1.606	1.118	1.795	−33.7	1.042	1.673	117.2
0 8 0	1.285	1.130	1.451	−32.3	1.035	1.329	120.9
0 6 0	0.963	1.133	1.091	−31.9	1.036	0.998	120.0

Table 2. *Group velocities in TSCC at* 123 K *from edges of phonon emission* ($\varepsilon = +1$) *and absorption* ($\varepsilon = -1$) *in TOF scans along the a direction*

$\theta = 44.8°$, $\Delta\theta = -3.22°$

		$\varepsilon = +1$			$\varepsilon = -1$		
hkl	v_n (km s^{-1})	β_g	c_g (km s^{-1})	$\zeta + \alpha$	β_g	c_g (km s^{-1})	$\zeta + \alpha$
6 0 0	1.840	1.141	2.099	−31.1	1.037	1.909	119.3
4 0 0	1.226	1.086	1.331	−38.2	1.033	1.266	125.9

(Schofield & Willis, 1987). Around the 040 reflection, which belongs to the third region ($c_g \cos\theta > v_n$), only weak edges occur.

Discussion

The results show that, in the TOF neutron diffraction studies of SBN and TSCC, the TDS in the vicinity of the Bragg peak is well described by the theory. Because in the theoretical approach the dispersion of the phonon velocity is not taken into account, discrepancies from theoretical predictions occur for higher q values.

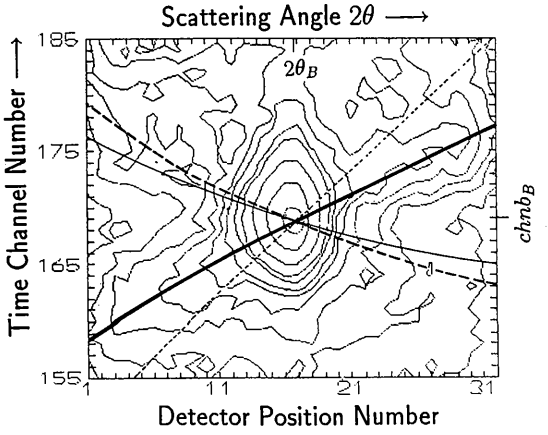

Fig. 5. Contour plot of the 0,16,0 reflection of TSCC around $2\theta_B = 89.6°$ measured at RT in the [001] zone (2θ range 83.7–95.5°; $ch_w = 64\,\mu s$). The curves (solid and broken lines) are the positions of the edges recalculated using equation (36) of Willis (1986) and checked using equation (64) of Schofield & Willis (1987) for the values $c_g^{high} = 3.45\,km\,s^{-1}$ and $c_g^{low} = 2.70\,km\,s^{-1}$, respectively. Two phonon groups are required to fit adequately the edge positions for absorption as well as emission (bold-faced curves).

In the case of the (nearly) elastically isotropic SBN, the measured phonon propagation velocity was about 8% smaller than the calculated phase velocity. However, the accuracy of this value is limited by the uncertainty of the elastic constant and, because it was determined by extrapolation of the slope of the phonon branch to small q's (Prokert, 1982), the uncertainty of c_{44} is about 8%, too. Thus, the value of $c_s = 2.9\ (5)$ km s^{-1}, which comes from the evaluation of the TDS, is much more accurate. The intensity differences of the TDS for the separated regions of phonon emission and absorption are displayed by the shape of the intensity distribution around the Bragg peak. The observed relations qualitatively agree with the expectations. The same is found for the changes of the intensity distribution with temperature. However, at the interpretation of the temperature dependence of the TDS, one should take into account that the phonon contribution itself and the diffuse scattering coming from structural disorder and lattice distortions may be changed by the occurrence of structural PT's (Balagurov, Prokert & Savenko, 1987; Prokert, Balagurov, Sangaa & Savenko, 1991). For these reasons, only rough estimations were made.

The analysis of the data from the TSCC single crystal requires more detailed inspection for two reasons: the elastic anisotropy of the material and the relatively high incoherent background in the TDS pattern. Nevertheless, consistent results were obtained by the evaluation of the edge positions at various scattering angles.

Along the a and b axes, which are extremal directions of the phase velocity, group and phase velocities coincide and from the elastic constant c_{66} one calculates a value of $c_s = 2.043$ km s^{-1} for the pure transverse mode. From the fact that the measured values of c_g along some of the measured nonsymmetry directions exceed this calculated value, it follows that the quasi-transverse mode must have higher velocities due to 'mode mixing'. The

velocities of the pure longitudial modes along a and b are 4.9 and 5.25 km s^{-1}, respectively.

The group velocities compiled in Tables 1 and 2 give information only for nonsymmetry propagation directions. For both of the listed phonon groups, which belong to different wave vectors, a striking variation of c_g was obtained. Whereas the first group (c_g^{high}) shows an expected angular dependence with the tendency to reach low group velocities around the [110] direction, the second one (c_g^{low}), obtained from edges around $0k0$ reflections, presents a surprising high change of c_g for the small angular changes. The behaviour is not understood so far and one may speculate about the effect of phonon focusing in elastically anisotropic crystals in which thermal-phonon group velocities tend to aggregate more around some directions than others. It depends on the curvature of the inverse phase velocity surface and is a common feature in many crystals (Every, 1980). On the other hand, the effect could originate from a violation of the validity condition of the theory owing to greater q values. This conjecture is supported by the calculated wave vectors of the second group, which are by far higher than those of the first group.

Along the b axis, scans were measured at RT as well as some degrees above and below the ferroelectric PT. Except for a slightly reduced intensity in the TDS patterns of the scans at low temperatures, no characteristic changes (*e.g.* owing to the piezoelectricity in the polar phase) were found within the limits of the given experimental resolution.

This work has been supported in part by the BMFT under registration sign 03-GO3ROS-5.

References

BALAGUROV, A. M., PROKERT, F. & SAVENKO, B. N. (1987). *Phys. Status Solidi A*, **103**, 131–144.

CARLILE, C. J., KEEN, D. A., WILSON, C. C. & WILLIS, B. T. M. (1992). *Acta Cryst.* A**48**, 826–829.

CARLILE, C. J. & WILLIS, B. T. M. (1989). *Acta Cryst.* A**45**, 708–715.

EVERY, A. G. (1980). *Phys. Rev. B*, **22**, 1746–1760.

LIU, S. T. (1978). *Ferroelectrics*, **22**, 709–713.

LIU, S. T. & CROSS, L. E. (1977). *Phys. Status Solidi A*, **41**, K83–K87.

PROKERT, F. (1982). *Phys. Status Solidi B*, **113**, 239–252.

PROKERT, F., BALAGUROV, A. M., SANGAA, D. & SAVENKO, B. N. (1991). *Ferroelectrics*, **124**, 121–126.

PROKHOROVA, S. D., SMOLENSKY, G. A., SINY, I. G., KUZMINOV, E. G., MIKVABIA, V. D. & ARNDT, H. (1980). *Ferroelectrics*, **25**, 629–632.

SAWADA, A., MAKITA, Y. & TAKAGI, Y. (1977). *J. Phys. Soc. Jpn*, **42**, 1918–1923.

SCHOFIELD, P. & WILLIS, B. T. M. (1987). *Acta Cryst.* A**43**, 803–809.

WILLIS, B. T. M. (1986). *Acta Cryst.* A**42**, 514–525.

WILLIS, B. T. M., CARLILE, C. J., WARD, R. C., DAVID, W. I. F. & JOHNSON, M. W. (1986). *Europhys. Lett.* **2**, 767–774.

Acta Cryst. (1995). A**51**, 129–134

Crystallography, Geometry and Physics in Higher Dimensions. XV. Reducible Crystal Families of Six-Dimensional Space

BY R. VEYSSEYRE, D. WEIGEL AND T. PHAN

Laboratoire de Chimie-Physique du Solide (unité associée au CNRS n° 453) et Département de Mathématiques, Ecole Centrale Paris, Grande Voie des Vignes, 92295 Châtenay-Malabry CEDEX, France

(*Received* 20 *April* 1994; *accepted* 18 *July* 1994)

Abstract

This paper and the following one of the series deal with the counting and the construction of the crystal families of Euclidean space E^6; this paper deals with the geometrically Z-reducible (gZ-red.) crystal families and paper XVI deals with the geometrically Z-irreducible (gZ-irr.) crystal familes. The method explained in previous papers for the construction of crystal families of Euclidean space E^5 has been adopted; for the reader's convenience, the main lines of this method are recalled. The method depends on two basic elements, namely, all the splittings of space E^6 into two-by-two orthogonal subspaces and the list of the gZ-irr. crystal families of one- to five-dimensional spaces. Besides the counting of the crystal families, this new geometrical method gives the names of these families and both the symbols and orders of their holohedries. The name of the crystal family directly introduces its 'conventional'-cell geometrical description and the various parameters (lengths and angles) defining the cell.

Introduction

In two previous papers (Veysseyre, Weigel & Phan, 1993; Weigel & Veysseyre, 1993), we introduced a general method for constructing the crystal families of Euclidean space E^n and emphasized the results for the crystal families of Euclidean spaces E^1 to E^5. This method is based on: (1) the consideration of every possible partition of space E^n into subspaces E^p, two-by-